Available online at www.sciencedirect.com
ScienceDirect
Journal of Molecular Catalysis A: Chemical 258 (2006) 104–112
JOURNAL OF MOLECULAR CATALYSIS A: CHEMICAL
www.elsevier.com/locate/molcata

Effects of pH on the microstructures and photocatalytic activity of mesoporous nanocrystalline titania powders prepared via hydrothermal method

Jiaguo Yu *, Yaorong Su, Bei Cheng, Minghua Zhou

State Key Laboratory of Advanced Technology for Material Synthesis and Processing, Wuhan University of Technology, Luoshi Road 122#, Wuhan 430070, PR China

Received 4 April 2006; accepted 15 May 2006
Available online 21 June 2006

Abstract

Highly photoactive nano-sized TiO_2 powder photocatalyst was prepared by a hydrothermal method at 180 °C for 5 h using tetrabutyl titanate (TBOT) as the precursor. The pH values of the starting suspensions were adjusted from 1 to 11 using a 1.0 M HCl or 1.0 M $NH_3 \cdot H_2O$ solution. The obtained TiO_2 powders were characterized with X-ray diffraction (XRD), N_2 adsorption–desorption measurement, transmission electron microscopy (TEM), X-ray photoelectron spectra, Fourier transform infrared (FTIR), Raman spectra and UV–vis spectrophotometry. The photocatalytic activity was evaluated by photocatalytic oxidation decomposition of acetone in air. The results showed that the pH values of the solutions obviously influenced the microstructures and photocatalytic activity of the as-prepared TiO_2 powders. With increasing pH values, the crystallization enhanced, crystallite size increased and BET specific surface areas decreased. The photocatalytic activity of TiO_2 powders prepared at a pH range of 6–9 exceeded that of Degussa P-25 by a factor of more than two times.

Keywords: Titania; Preparation; Hydrothermal reaction; pH; Microstructure; Photocatalytic activity; Mesoporous; Nanocrystalline

1. Introduction

To solve the increasingly serious problems of environmental pollutions, a great deal of effort has been made in recent years, and various catalytic techniques are being applied in the fields of environmental protection. Photocatalysis is one technique that has great potential to control aqueous organic contaminates or air pollutants. It is believed to have several advantages over conventional oxidation processes, such as: (1) complete mineralization of the pollutants; (2) use of the near-UV or solar light; (3) no addition of other chemicals; (4) operation at near room temperature [1–6]. Although photocatalytic degradations of trace toxic organic compounds in water or air have been investigated intensively in the past decade, there still remain some problems in practical applications [5]. Fundamental research regarding the preparation of photocatalyst with highly photocatalytic activity, the immobilization of powder photocatalyst, and the improvement of photocatalyst performance are priorities to be considered [5–7].

Among various oxide semiconductor photocatalysts, titania has been proven to be the most suitable for widespread environmental applications for its strong oxidizing power, non-toxicity, long-term photostability and cost effectiveness. Titania has three crystalline phases: rutile, anatase and brookite, among which, rutile is a thermodynamic stable state while the latter two phases are metastable state [8], and anatase is generally recognized to be the most active phase as opposed to the rutile and brookite forms. Usually, the photocatalytic activity of titania depends on its crystal phase, crystallite size, crystallization, specific surface areas, pore structures and so on. For example, many studies have confirmed that the anatase phase of titania is a good photocatalytic material due to its low recombination rate of photogenerated electrons and holes [9,10]. Moreover, we found that the composite of two phases of titania was more beneficial for suppressing the recombination of photo-generated electrons and holes and thus enhanced the photocatalytic activity [9].

* Corresponding author.
E-mail address: jiaguoyu@yahoo.com (J. Yu).

1381-1169/$ – see front matter © 2006 Elsevier B.V. All rights reserved.
doi:10.1016/j.molcata.2006.05.036

The chemical and physical properties of titania photocatalysts depend also on the procedures and conditions of preparation. A few methods, such as hydrolysis (chemical precipitation) [11], reverse micelles (microemulsion) [12,13], sol–gel [14,15], and liquid phase deposition [16], have been used to prepare TiO_2 nanocrystalline photocatalyst. Comparing with these methods, the hydrothermal method has more advantages [12,13]: (1) Crystallization temperature for anatase phase is below 200 °C. (2) By changing hydrothermal conditions (such as temperature, time, reactant concentration, additives, etc.), various crystalline products with different composition, structure and morphology could be obtained. (3) Low energy consumption and environmentally friendly process. (4) The equipment and processing required are simpler, and the control of reaction conditions is easier, etc. So the hydrothermal synthesis should be a good method for the preparation of semiconductor photocatalyst and other oxide ceramic fine powders.

In this work, highly photoactive mesoporous nanocrystalline TiO_2 powder photocatalysts were prepared by a simple hydrothermal method at 180 °C for 5 h at different pH. The effects of initial pH values on the microstructures and photocatalytic activity of mesoporous titania powders were investigated and discussed.

2. Experimental

2.1. Preparation

All chemicals used in this study were used as received from Shanghai Chemical Regent Factory of China without further purification. Distilled water was used in all experiments.

Tetrabutyl titanate ($Ti(OC_4H_9)_4$, TBOT) was used as a titanium source. The pH values of the distilled water were adjusted to pH 1, 3, 6, 9 and 11 using a 1.0 M HCl or 1.0 M $NH_3{\cdot}H_2O$ aqueous solution. Then, 13.2 ml of TBOT was added dropwise into 135 ml of the above solution under vigorous stirring for 2 h. The obtained slurry was re-adjusted to the initial pH values by the above method, and then the slurry was placed into a 200 ml stainless steel autoclave with a Teflon liner. The autoclave was incubated at 180 °C for 5 h and then cooled to room temperature. After reaction, the pH value of the solution almost kept unchanged. The white precipitate was filtrated and washed with distilled water for five times. The obtained samples were dried at 100 °C in a vacuum oven for 10 h and then ground to fine powders with an agate mortar.

2.2. Characterization

The X-ray diffraction (XRD) patterns obtained on an X-ray diffractometer (type HZG41B-PC) using Cu Kα radiation at a scan rate of 0.05° $2\theta\,s^{-1}$ used to characterize the crystalline phase and crystallite size of the TiO_2 powders. The accelerating voltage and the applied current were 15 kV and 20 mA, respectively. The phase content of a sample can be calculated from the integrated intensities of anatase (1 0 1), rutile (1 1 0) and brookite (1 2 1) peaks. If the sample contains anatase and brookite phases, the mass fraction of brookite can be calculated according to Eq. (1) [17–20].

$$W_B = \frac{2721A_B}{0.886A_A + 2721A_B} \quad (1)$$

where A_A and A_B represent the integrated intensity of the anatase (1 0 1) and brookite (1 2 1) peaks, respectively. With Eq. (1), the phase contents of anatase and brookite in TiO_2 samples can be calculated. The average crystallite sizes of anatase and brookite were determined according to the Scherrer equation using the FWHM data of each phase after correcting the instrumental broadening [17–20]. X-ray photoelectron spectroscopy (XPS) measurements were performed on the ESCALAB-210 spectrometer (Thermo VG Scientific, UK) with Mg Kα source. All the binding energies were referenced to the C 1s peak at 285.0 eV of the surface adventitious carbon. Transmission electron microscopy (TEM) and high-resolution transmission electron microscopy (HRTEM) images, which were obtained using a JEOLTEM-2010F at an acceleration voltage of 200 kV, were used to observe or determine the morphology, size and identity of nanocrystal particles in the as-prepared TiO_2 powders. The UV–vis spectra were obtained by an UV–vis spectrophotometer (UV-2550, Shimadzu, Japan). Infrared (IR) spectra on pellets of the samples mixed with KBr were recorded on a Nicolet Magna 560 FTIR spectrometer at a resolution of 4 cm^{-1}. The concentration of the samples was kept at about 0.25–0.3%. The Brunauer–Emmett–Teller (BET) surface area (S_{BET}) of the powders was analyzed by nitrogen adsorption in a Micromeritics ASAP 2020 nitrogen adsorption apparatus (USA). All the samples were degassed at 180 °C prior to nitrogen adsorption measurements. The BET surface area was determined by a multipoint BET method using the adsorption data in the relative pressure (P/P_0) range of 0.05–0.3. Desorption isotherm was used to determine the pore size distribution via the Barret–Joyner–Halender (BJH) method with cylindrical pore size [21]. The nitrogen adsorption volume at the relative pressure (P/P_0) of 0.994 was used to determine the pore volume and average pore size.

2.3. Measurement of photocatalytic activity

Acetone (CH_3COCH_3) is a common chemical that is used extensively in various industrial and domestic applications. Therefore, we chose it as a model contaminate chemical. Photocatalytic oxidation of the acetone is based on the following reaction [22–25]:

$$CH_3COCH_3 + 4O_2 \rightarrow 3CO_2 + 3H_2O \quad (2)$$

The photocatalytic activity measurements of the as-prepared TiO_2 powders and Degussa P-25 for the oxidation of acetone in air were performed at ambient temperature using a 15 l photocatalytic reactor, followed by the photodegradation of acetone with an initial concentration of 400 ± 20 ppm. The detailed experimental setup and process have been reported elsewhere [25]. The TiO_2 photocatalysts were prepared by coating an aqueous suspension of TiO_2 samples onto four dishes with a diameter of 7.0 cm. The dishes containing catalysts were dried at 100 °C and then cooled to room temperature before being used. The

weight of the TiO_2 catalysts used for each experiment was kept at 0.3 g. After the catalysts were placed in the reactor, a small amount of acetone was injected with a syringe. The reactor was connected to a $CaCl_2$-containing dryer used for controlling the initial humidity in the reactor. The acetone vapor was allowed to reach adsorption–desorption equilibrium with catalysts in the reactor prior to UV light irradiation. A 15 W UV lamp with a primary wavelength at 365 nm provided illumination and its intensity striking on the coating measured with a UV radiometer (Model: UV-A, made in Photoelectric Instrument Factory of Beijing Normal University) was 2.5 mW cm^{-2}. The concentration analysis of acetone, carbon dioxide, and water vapor in the reaction was conducted on line with a Photoacoustic IR Multigas Monitor (INNOVA Air Tech Instruments Model 1312). Each set of experiment was followed for 60 min. The photocatalytic activity of the TiO_2 samples can be quantitatively evaluated by comparing the apparent reaction rate constants. The photocatalytic oxidation of acetone is a pseudo-first-order reaction and its kinetics may be expressed as follows: $\ln(C_0/C) = kt$ [26], where k is the apparent reaction rate constant, C_0 and C are the initial concentration and the reaction concentration of acetone, respectively. The photocatalytic activity of Degussa P-25 powders was also measured as a reference to compare with that of the as-prepared catalysts. The measurements were repeated for each catalytic system for three times, and the experimental error was found to be within ±5%.

3. Results and discussion

3.1. Crystal structure

XRD was used to investigate the changes of phase structure of the as-prepared TiO_2 powders at various pH values. Fig. 1 shows XRD patterns of the as-synthesized TiO_2 powders at different pH value. At $pH \leq 6$, TiO_2 powders contained two phases. The anatase was main phase and brookite was minor phase. A small peak at $2\theta = 30.7^\circ$ corresponded to the (1 2 1) diffraction peak of brookite phase. The presence of this phase caused the slight shift to a higher angle of the anatase (1 0 1) peak since there was an overlapping brookite (1 2 0) and (1 1 1) peaks [27]. With increasing pH values, the intensities of anatase diffraction peaks steadily became stronger, and meanwhile the

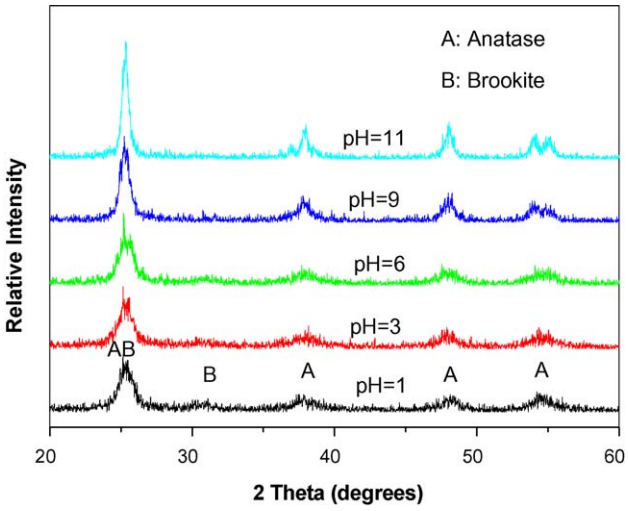

Fig. 1. XRD patterns of the as-synthesized TiO_2 powders at different pH values.

intensities of brookite diffraction peaks decreased gradually and ultimately disappeared. At pH 9 and 11, the TiO_2 powders only appeared anatase phase. However, the width of the main peak of the anatase became narrower with increasing the pH. This indicated the formation of greater crystallites. Our results suggested that a weak acid condition or a low pH value was favorable to the formation of brookite, while weak basic condition favored the formation of pure anatase. The average crystallite size of TiO_2 powders was calculated by line broadening methods and equation proposed by Scherrer. The results are shown in Table 1.

The formation of brookite phase in acid conditions could be explained as follows: When TBOT was added into a HCl or $NH_3{\cdot}H_2O$ solution, hydrolysis reaction occurred leading to the formation of $Ti(OH)_x(OC_4H_9)_{4-x}$ by the following reaction:

$$Ti(OC_4H_9)_4 + x(OH^-) \rightarrow Ti(OH)_x(OC_4H_9)_{4-x} + x(C_4H_9O^-) \quad (3)$$

where x was related to the pH value of the starting solution. The higher the pH value was, the bigger the value of x. In a HCl solution, the ligand field strength of Cl^- ions was larger than that of butoxy group, so Cl^- ions could substitute the butoxy groups in the $Ti(OH)_x(OC_4H_9)_{4-x}$ complex, and then

Table 1
Effects of pH values on physicochemical properties of TiO_2 powders

pH	Crystallite size[a] (nm)	Phase content[b] (%)	Relative crystallinity[c]	S_{BET}[d] ($m^2\ g^{-1}$)	Pore volume[e] ($cm^3\ g^{-1}$)	Pore size[f] (nm)
1	7.7 (A)	58.5 (A), 41.5 (B)	1	185.8	0.319	6.98
3	8.9 (A)	63 (A), 37 (B)	1.0	183.0	0.314	6.77
6	10.2 (A)	70 (A), 30 (B)	1.2	179.4	0.311	6.93
9	13.3 (A)	100 (A)	1.6	127.3	0.288	9.05
11	20.3 (A)	100 (A)	2.3	81.1	0.293	14.47

A and B denote anatase and brookite, respectively.
[a] Calculated by XRD using the Scherrer equation.
[b] Determined by XRD method.
[c] Calculated from the relative intensity of the diffraction peak of anatase (1 0 1) plane (reference: the sample prepared at pH 1).
[d] BET surface area calculated from the linear part of the adsorption isotherm ($P/P_0 = 0.1$–0.2).
[e] Total pore volume, taken from the volume of N_2 adsorbed at $P/P_0 = 0.995$.
[f] Average pore diameter, estimated using the desorption branch of the isotherm and the Barret–Joyner–Halender (BJH) method.

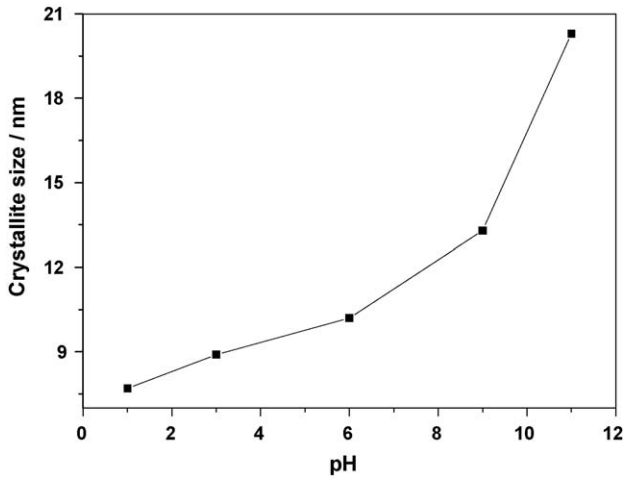

Fig. 2. Influence of pH values on average crystallite size of nanocrystalline TiO_2 powders.

the complex $Ti(OH)_2Cl_2$ formed. According to ligand field theory, Ti(IV)($3d^0$) complex ions are all octahedrally coordinated in solution and crystal. Hence, the complex $Ti(OH)_2Cl_2$ actually existed in the form of $Ti(OH)_2Cl_2(H_2O)_2$ in a solution. Pottier et al. reported that $Ti(OH)_2Cl_2(H_2O)_2$ could be the precursor of brookite [28]. This mechanism was favored to explain the occurrence of brookite in the samples. Moreover, the higher the concentration of Cl^- ions in the solution, the more the complex $Ti(OH)_2Cl_2(H_2O)_2$, and so the greater the content of brookite in the sample. This was in good accordance with our experiment results.

Fig. 2 shows the influence of pH values on average crystallite size of nanocrystalline TiO_2 powders. The results indicated that the average crystallite size of the samples was strongly dependent on the pH values of the precipitation medium. The average crystallite size increased with increasing the pH values. This is probably due to the fact that when the pH of the precipitation medium was low, the quantity of the hydroxyl groups in it was small, which limited the hydrolysis of alkoxide, and unhydrolyzed alkyls and Cl^- ions remained in the precursors, which prevented the crystallization of the samples and the growth of the TiO_2 crystallites. With increasing the pH value, the quantity of the hydroxyl groups in the precipitation medium increased and the hydrolysis of alkoxides were enhanced, and accordingly the amount of unhydrolyzed alkyls remained in the precursor decreased. The less the unhydrolyzed alkyls remained in the precursor, the better the crystallization of TiO_2 and the greater the crystallite size.

3.2. TEM study

Fig. 3(a) and (b) show TEM and HRTEM images of the TiO_2 powders prepared at pH 9, respectively. It could be observed from Fig. 3(a) that the nanocrystallite showed an agglomerated status, and mesoporous structures without a long-range order. The size of the primary particles estimated from the TEM images was about 13 ± 1 nm, which was in good agreement with the value (13.3 nm) calculated from XRD pattern using the Scherrer equation. Fig. 3(b) shows the corresponding HRTEM image of the sample. It shows clear lattice fringes, which allowed for the identification of crystallographic spacing. The fringes of 0.35 nm matched that of the (1 0 1) crystallographic plane of TiO_2 anatase.

3.3. Raman spectroscopy

Further insights into the phase composition of the samples prepared in various pH values could be obtained from micro-Raman spectroscopy. This technique allows selecting a sampled area of several micrometers in size, and by scanning the sample surface, we can distinguish different Raman-active phases in the samples. Fig. 4 displays representative Raman spectra of the samples prepared at different pH values. Using these spectra, we could identify the Raman bands of anatase at 145 cm^{-1} (E_g), 398 cm^{-1} (B_{1g}), 516 cm^{-1} (B_{1g}) and 639 cm^{-1} (E_g) for all samples [29,30], especially for the samples obtained at pH 9 and 11, which contained only anatase phase. Besides, the clear Raman bands at 243 cm^{-1} (A_{1g}), 325 cm^{-1} (B_{1g}) and 365 cm^{-1} (B_{2g}) observed in the pH 1 sample were characteristic vibrations of brookite [31,32], which demonstrated that it contained anatase and brookite phases. The above results coincided with the XRD results. Further observation showed that with increasing the pH value from pH 1 to 11, the wavenumbers of all peaks decreased

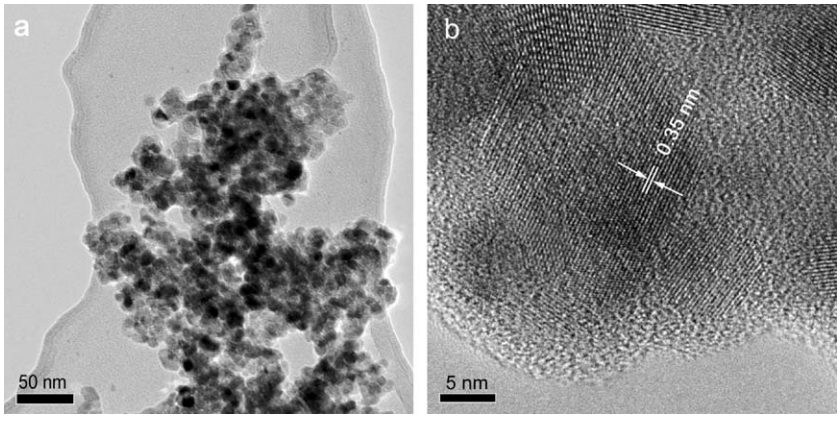

Fig. 3. TEM and HRTEM images of the TiO_2 powders prepared at pH 9.

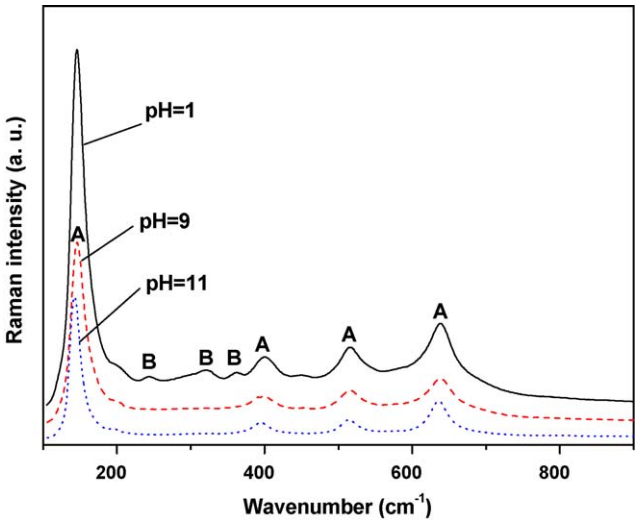

Fig. 4. Raman spectra of the TiO_2 powders prepared at pH 1, 9 and 11.

slightly. The shift of the Raman peaks to lower wavenumbers with increasing the pH value could be attributed to the increase of crystallite size and the particle size effect [13].

3.4. FTIR spectra

The FTIR spectra of the samples prepared at pH 1, 9 and 11 are shown in Fig. 5. It is believed that the broad peak at 3400 and the peak at 1650 cm^{-1} correspond to the surface-adsorbed water and hydroxyl groups. Obviously, with increasing the pH values, the surface-adsorbed water and hydroxyl groups decreased slightly. This was due to the decrease of specific surface areas (as shown in Table 1), which caused the reduction of the adsorbed water. The main peak at 400–700 cm^{-1} was attributed to Ti–O stretching and Ti–O–Ti bridging stretching modes [33]. Besides, two weak bands at 2924 and 2854 cm^{-1} (ν_{CH} and ν_{CH_2}) in the as-synthesized TiO_2 powders could be attributed to the characteristic frequencies of residual organic species, which is not completely removed by distilled water washing [34]. Further observation indicated that the peaks at 2924 and 2854 cm^{-1} almost disappeared for the sample prepared at pH 1. This could be attributed to the fact that Cl^- ions could substitute the unhydrolysis butoxy groups in the $Ti(OH)_x(OC_4H_9)_{4-x}$ complex, and then formed the complex $Ti(OH)_2Cl_2$ [28], resulting in the disappearance of the peaks at 2924 and 2854 cm^{-1}. The small peaks at 1380–1400 cm^{-1} region could be ascribed to carboxyl (C=O) groups [35]. The carboxyl groups might be resulted from the oxidation of the organic species during the hydrothermal treatment.

3.5. BET surface areas and pore distribution

Fig. 6 shows nitrogen adsorption–desorption isotherms of the TiO_2 powders prepared at pH 1, 9 and 11. The isotherm of the pH 1 sample was of type IV (BDDT classification) [21] and had two hysteresis loops, indicating a bimodal pore size distribution in the mesoporous region. The shapes of two hysteresis loops were different from each other. At a low relative pressure range between 0.4 and 0.8, the hysteresis loop was of type H_2, which could be observed in the pores with narrow necks and wider bodies (ink-bottle pores) [21]. However, at a high relative pressure range between 0.8 and 1.0, the shape of the hysteresis loop was of hype H_3 associated with aggregates of plate like particles giving rise to slit-like pores [21]. The isotherms of the samples obtained at pH 9 and 11 were also of types IV (BDDT classification). At high relative pressures from 0.5 and 1.0, the isotherms exhibited hysteresis loops of type H_3, indicating that the powders contained mesopores (2–50 nm). With increasing the pH, the hysteresis loops shifted to a higher relative pressure region and the areas of the hysteresis loops gradually became small.

Fig. 7 shows the corresponding pore size distribution curves of the TiO_2 powders prepared at pH 1, 9 and 11. The powders prepared at pH 1 showed a bimodal pore size distributions consisting of fine intra-aggregated pores with a maximum pore diameters of 5.4 nm and larger inter-aggregated pores with a maximum pore diameters of 30 nm [10]. According to Kumar et al. [36], the

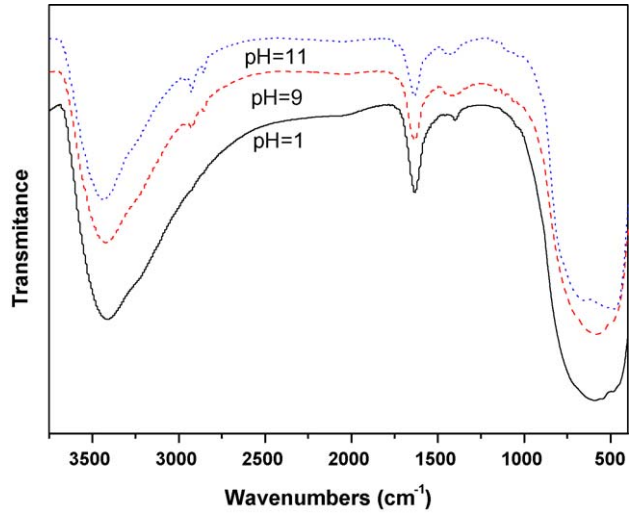

Fig. 5. FTIR spectra of the TiO_2 powders prepared at pH 1, 9 and 11.

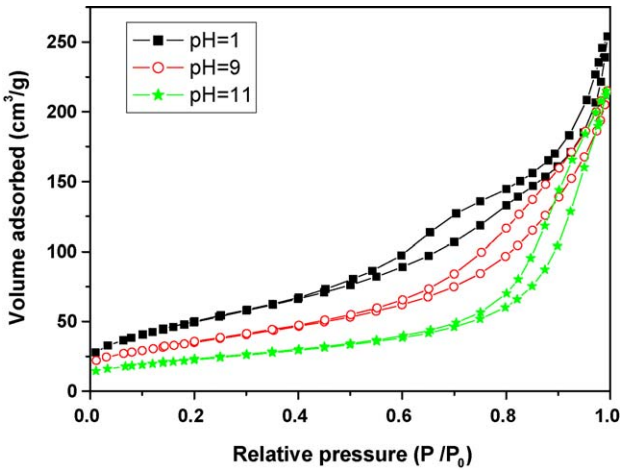

Fig. 6. Nitrogen adsorption–desorption isotherms of the TiO_2 powders prepared at pH 1, 9 and 11.

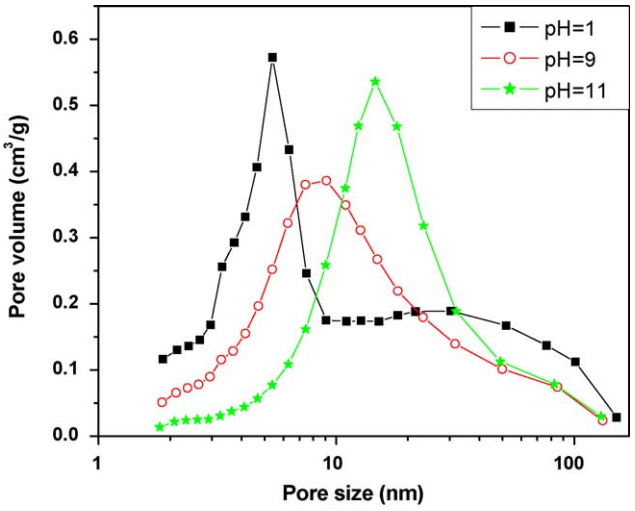

Fig. 7. Pore size distribution curves of the TiO_2 powders prepared at pH 1, 9 and 11.

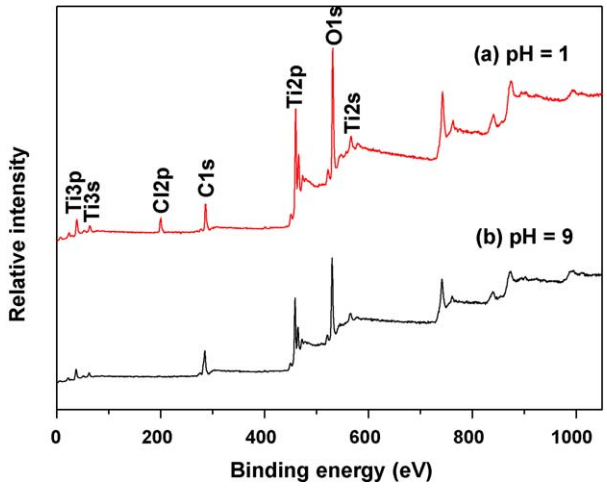

Fig. 8. XPS survey spectra of the TiO_2 powders prepared at (a) pH 1 and (b) pH 9.

bimodal pore size distribution arose from the hard aggregated in the powders. In addition, they reported that there were two types of pores on the bimodal pore size distribution. One was the fine intra-aggregated pore (represented by the hysteresis loop in the lower P/P_0 range) and the other was the larger inter-aggregated pore (hysteresis loop in the higher P/P_0 range). At pH 9 and 11, the maximum pore sizes of the intra-aggregated pores shifted into larger mesopores regions (ca. 9 and 14.5 nm, respectively), indicating the growth of pores. This was caused by the enhancement of the crystallization of the TiO_2 powders and the growth of the anatase crystallites (as shown in Table 1). With increasing the pH values (at pH 9 and 11), the pore gradually became a monomodal distribution probably due to the overlapping of the fine intra-aggregated pore and the larger inter-aggregated pore.

Table 1 shows the influences of pH values on the physical and chemical properties of the as-prepared TiO_2 powders. It could be seem from Table 1 that the pH 1 powders showed a large specific surface area, and its value reached 185.0 $m^2\ g^{-1}$. With increasing the pH values, the BET specific surface areas decreased slightly. This might be due to the increase in the crystallite sizes of the prepared TiO_2 powders.

3.6. XPS study

Fig. 8 shows the XPS survey spectra of the TiO_2 powders prepared at pH 1 and 9. It could be seen that the TiO_2 powders prepared at pH 9 only contained Ti, O and C elements, with sharp photoelectron peaks appearing at binding energies of 458 (Ti 2p), 531 (O 1s) and 285 eV (C 1s). However, the sample obtained at pH 1 not only contained Ti, O and C, but also a small amount of Cl element (binding energy at 199 eV), which might come from the Cl element in complex $Ti(OH)_2Cl_2(H_2O)_2$ (as mentioned above), and/or HCl. The atomic ratios of Ti to O of both samples were in good agreement with the nominal atomic composition of TiO_2. The carbon peak was attributed to the residual carbon from the sample and adventitious hydrocarbon from XPS instrument itself. Fig. 9(a) and (b) show the corresponding high-resolution XPS spectra of the O 1s region taken on the surface of the sample prepared at pH 1 and 9, respectively. The O 1s region could be fitted into two peaks. The main peak was ascribed to the Ti–O bonds in TiO_2. The minor peak was due to the hydroxyl groups [25]. It was interesting to note that the peak area of hydroxyl groups of the pH 1 sample was larger than that of the pH 9 sample, indicating that the former contained more hydroxyl groups due to its large specific surface areas (as shown in Table 1). Fig. 10 shows the corresponding high-resolution XPS spectra of C 1s region of the above two samples. The C 1s region of the pH 9 sample could be fitted into three smaller peaks. The main peak at about 285.0 eV corresponded to carbons of saturated hydrocarbon groups ($–CH_3$, $–CH_2–$) [37], which came from the residual carbon in the sample or adventitious hydrocarbon from XPS instrument itself. The other two peaks at about 282 and 289 eV were ascribed to Ti–C bonds [38] and C=O double bonds [39], respectively. Of course, their formation mechanism still needed to be further investigated. However,

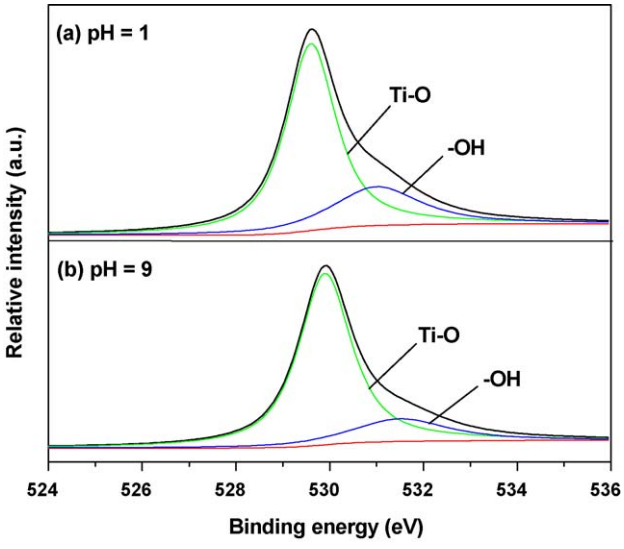

Fig. 9. High-resolution XPS spectra of O 1s region of the TiO_2 powders prepared at (a) pH 1 and (b) pH 9.

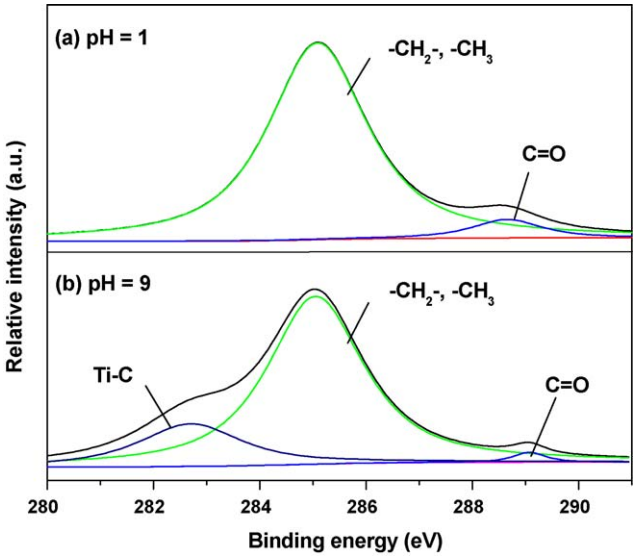

Fig. 10. High-resolution XPS spectra of C 1s region of the TiO_2 powders prepared at (a) pH 1 and (b) pH 9.

no Ti–C peak was observed for the pH 1 sample, implicating that Cl^- ions could completely substitute the un-hydrolysis butoxy groups in the $Ti(OH)_x(OC_4H_9)_{4-x}$ complex. This also supported and confirmed the explanation of the above FTIR results.

3.7. UV–vis spectra

The influences of pH values on the light absorption characteristics of TiO_2 powders are shown in Fig. 11. A significant increase at wavelengths shorter than 390 nm could be attributed to absorption of light caused by the excitation of electrons from the valence band to the conduction band of TiO_2. The TiO_2 powders prepared at pH 3 and 9 showed a stronger absorption in the 250–300 nm range and a blue shift in the band gap transition as compared with the TiO_2 powders of pH 11. The differences in adsorption were attributed to the change of crystallite size and phase structure.

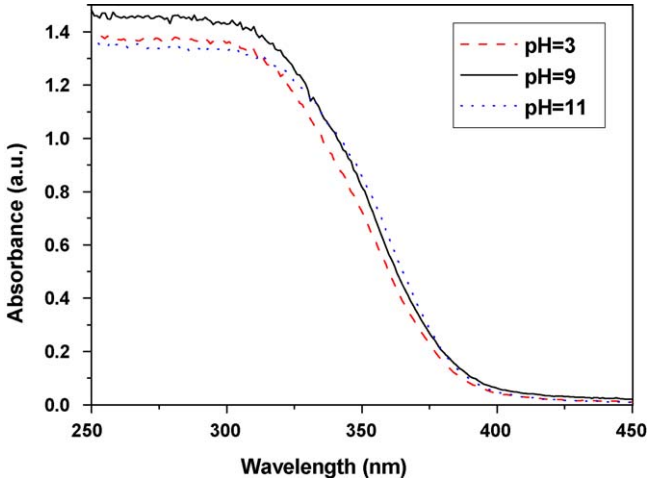

Fig. 11. UV–vis absorption spectra of TiO_2 powders prepared at pH 3, 9 and 11.

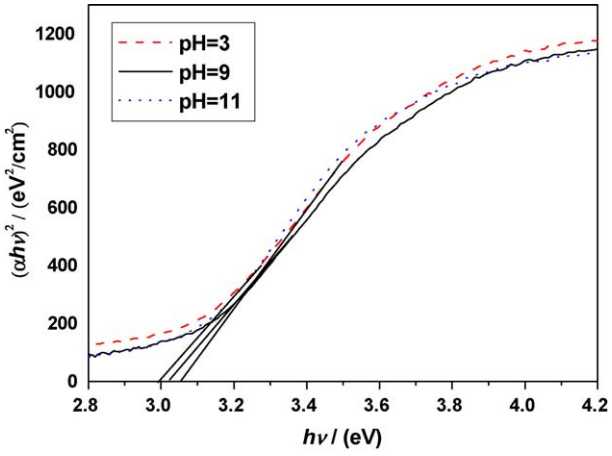

Fig. 12. Plots of $(\alpha h\nu)^2$ vs. $h\nu$ for the as-prepared TiO_2 powders prepared at pH 3, 9 and 11.

The adsorption edges shifted toward shorter wavelengths for the TiO_2 powders prepared at pH 3 and 9. This clearly indicated an increase in the band gap energy of TiO_2. Band gap energy could be estimated from a plot of $(\alpha h\nu)^2$ versus photon energy ($h\nu$). The intercept of the tangent to the plot would give a good approximation of the band gap energy for TiO_2 [40]. The adsorption coefficient α could be calculated from the measured adsorbance (A) using the following equation:

$$\alpha = \frac{2.303\rho \times 10^3}{lcM} A \quad (4)$$

where the density $\rho = 3.9\,\mathrm{g\,cm^{-3}}$, molecular weight $M = 79.9\,\mathrm{g\,mol^{-1}}$, c the molar concentration of TiO_2, and l is the optical path length [41].

Plots of $(\alpha h\nu)^2$ versus photon energy ($h\nu$) for TiO_2 powders prepared at pH 3, 9 and 11 are shown in Fig. 12. The band gap energies estimated from the intercept of the tangents of the plots were 3.06, 3.02 and 3.0 eV for the samples of pH 3, 9 and 11, respectively. The band gap of the powders prepared at pH 3 and 9 was larger than that of the sample prepared at pH 11, this might be assigned to the existence of brookite phase in the sample of pH 3 and smaller crystallite size. Mo and Ching reported that the direct band gap of brookite was 0.16 eV larger than that of anatase [42]. Hence, the band gap of the anatase–brookite mixed phase would be larger than that of the pure anatase phase. This was in good agreement with our results. Of course, the TiO_2 powders with smaller crystallite size would exhibit a larger band gap due to quantum size effect [43]. These enough explained the above results.

3.8. Photocatalytic activity

Fig. 13 shows the dependence of the apparent rate constants ($k\,\mathrm{min^{-1}}$) on pH values of the starting solution. For TiO_2 powder prepared at pH 1 and dried at 100 °C for 10 h, it showed a good photocatalytic activity. Its k reached 2.65×10^{-3}. This was assigned to its high specific surface areas and small crystallite size. With increasing the pH, the photocatalytic activity of TiO_2 powder significantly increased due to the enhancement of crys-

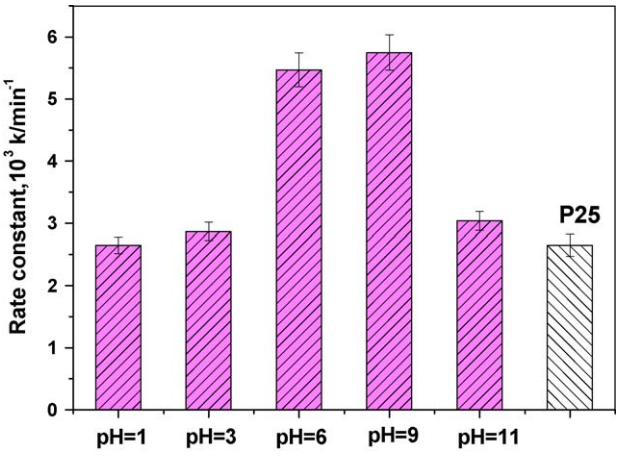

Fig. 13. The dependence of the apparent rate constants on pH values.

tallization of TiO_2 (as shown in Fig. 1 and Table 1). At pH 9, the k reached the highest value and its value was 5.75×10^{-3}. The k was determined to be 2.65×10^{-3} for Degussa P-25 (P25), which is well known to have a high photocatalytic activity. The photocatalytic activity of TiO_2 powders prepared at pH 9 exceeded that of P25 by a factor of 2.17, which might be attributed to the fact that the former had larger specific surface areas, smaller crystallite size and mesoporous structures, etc. Usually, the specific surface areas and crystallite size of P25 are about 50 $m^2\ g^{-1}$ and 30 nm, respectively. With further increasing the initial pH values, the k decreased drastically. This was due to the crystalline growth and drastic decrease in specific surface areas (as shown in Table 1) [44,45].

4. Conclusions

(1) The pH values of the starting solution had significant effect on the crystallinity, crystallite size, phase structure, and photocatalytic activity of the prepared TiO_2 powders by hydrothermal method. Weak acid conditions of the starting solution were in favor of the formation of brookite phase while basic conditions were favorable for the formation of pure anatase phase. With increasing the pH value, the crystallization enhanced, crystallite size increased and BET specific surface areas decreased.

(2) The photocatalytic activity of the TiO_2 powders prepared at pH 6 and 9 exceeded that of Degussa P-25 by a factor of more than two times. This might be ascribed to the fact that the samples prepared by this method had higher specific surface areas and smaller particle size.

(3) For the sample prepared at pH 1, the pore size distribution showed a bimodal distribution in mesoporous region: one was fine intra-aggregated pores with a maximum pore diameter of 5.4 nm and the other was larger inter-aggregated pores with a maximum pore diameter of 30 nm. With increasing the pH values (at pH 9 and 11), the pore gradually became a monomodal distribution probably due to the overlapping of the fine intra-aggregated pore and the larger inter-aggregated pore.

Acknowledgements

This work was partially supported by the National Natural Science Foundation of China (no. 20473059). This work was also financially supported by the Key Research Project of the Ministry of Education (no. 106114).

References

[1] M.R. Hoffmann, S.T. Martin, W. Choi, D.W. Bahnemann, Chem. Rev. 95 (1995) 69.
[2] A. Fujishima, T.N. Rao, D.A. Tryk, J. Photochem. Photobiol. C 1 (2000) 1.
[3] A.L. Linsebigler, G. Lu, J.T. Yates Jr., Chem. Rev. 95 (1995) 735.
[4] H. Tada, M. Yamamoto, S. Ito, Langmuir 15 (1999) 3699.
[5] J.A. Wang, R. Limas-Ballesteros, T. Lopez, A. Moreno, R. Gomez, O. Novaro, X. Bokhimi, J. Phys. Chem. B 105 (2001) 9692.
[6] F.B. Li, X.Z. Li, M.F. Hou, Appl. Catal. B 48 (2004) 185.
[7] J.G. Yu, J.C. Yu, W.K. Ho, Z.T. Jiang, New J. Chem. 26 (2002) 607.
[8] M. Gopal, W.J. Moberly Chan, L.C. De Jonghe, J. Mater. Sci. 32 (1997) 6001.
[9] J.C. Yu, J.G. Yu, W.K. Ho, L.Z. Zhang, Chem. Commun. (2001) 1942.
[10] J.G. Yu, J.C. Yu, M.K.P. Leung, W.K. Ho, B. Cheng, X.J. Zhao, J.C. Zhao, J. Catal. 217 (2003) 69.
[11] C.C. Wang, J.Y. Ying, Chem. Mater. 11 (1999) 3113.
[12] Y.T. Qian, Q.W. Chen, Z.Y. Chen, C.G. Fan, G.E. Zhou, J. Mater. Chem. 3 (1993) 203.
[13] H.M. Cheng, J.M. Ma, Z.G. Zhao, L.M. Qi, Chem. Mater. 7 (1995) 663.
[14] J.G. Yu, X.J. Zhao, Q.N. Zhao, Thin Solid Films 379 (2000) 7.
[15] F.B. Li, X.Z. Li, Appl. Catal. A 228 (2002) 15.
[16] J.G. Yu, H.G. Yu, B. Cheng, X.J. Zhao, J.C. Yu, W.K. Ho, J. Phys. Chem. B. 107 (2003) 13871.
[17] H. Zhang, J. Banfield, J. Phys. Chem. B 104 (2000) 3481.
[18] J.G. Yu, J.C. Yu, B. Cheng, S.K. Hark, K. Iu, J. Solid State Chem. 174 (2003) 372.
[19] J.G. Yu, J.C. Yu, B. Cheng, X.J. Zhao, Sci. China B 46 (2003) 549.
[20] J.G. Yu, J.C. Yu, Chin. J. Chem. 21 (2003) 994.
[21] K.S.W. Sing, D.H. Everett, R.A.W. Haul, L. Moscou, R.A. Pierotti, J. Rouquerol, T. Siemieniewska, Pure Appl. Chem. 57 (1985) 603.
[22] M.E. Zorn, D.T. Tompkins, W.A. Zeltner, M.A. Anderson, Appl. Catal. B 23 (1999) 1.
[23] M.H. Zhou, J.G. Yu, B. Cheng, H.G. Yu, Mater. Chem. Phys. 93 (2005) 159.
[24] J. Lin, J.C. Yu, D. Lo, S.K. Lam, J. Catal. 183 (1999) 368.
[25] J.C. Yu, J.G. Yu, J.C. Zhao, Appl. Catal. B 36 (2002) 31.
[26] J.G. Yu, M.H. Zhou, B. Cheng, H.G. Yu, X.J. Zhao, J. Mol. Catal. A 227 (2005) 75.
[27] J.C. Yu, J.G. Yu, W.K. Ho, Z.T. Jiang, L.Z. Zhang, Chem. Mater. 14 (2002) 3808.
[28] A. Pottier, S. Cassaignon, F. Villain, E. Tronc, J.P. Jolivet, J. Mater. Chem. 13 (2003) 877.
[29] S.P.S. Proto, P.A. Fleury, T.C. Damen, Phys. Rev. 154 (1967) 522.
[30] M. Gotić, M. Ivanda, S. Popvić, S. Musić, A. Sekulić, A. Turković, K. Furić, J. Raman Spectrosc. 26 (1997) 555.
[31] G.A. Tompsett, G.A. Bowmake, R.P. Cooney, J.B. Metson, K.A. Rodgers, J.M. Seakins, J. Raman Spectrosc. 26 (1995) 57.
[32] D.K. Arkhipenko, Y.S. Bobovich, M.Y. Tsenter, Zh. Prikl. Spektrosk. 40 (1984) 304.
[33] A.M. Peiro, J. Peral, C. Domingo, X. Momenech, J.A. Ayllon, Chem. Mater. 13 (2001) 2567.
[34] G.de. Sole-IIIia, A. Louis, C. Sanchez, Chem. Mater. 14 (2002) 750.
[35] S. Biniak, G. Szymanski, J. Siedlewski, A. Swiatkowski, Carbon 35 (1799) 810.
[36] K.N.P. Kumar, J. Kumar, K. Keizer, J. Am. Ceram. Soc. 77 (1994) 1396.
[37] B. Lindberg, R. Maripuu, K. Siegbahn, R. Larsson, C.G. Golander, J.C. Eriksson, J. Coll. Interf. Sci. 95 (1983) 308.

[38] C. Yeongsoo, T. Umebayashi, M. Yoshikawa, J. Mater. Sci. 69 (2004) 1837.
[39] M. Polovina, B. Babić, B. Kaluderović, A. Dekanski, Carbon 35 (1997) 1047.
[40] N. Serpone, D. Lawless, R. Khsirutdinov, J. Phys. Chem. 99 (1995) 16646.
[41] C. Kormann, D.W. Bahnemann, M.R. Hoffmann, J. Phys. Chem. 92 (1988) 5196.
[42] S.D. Mo, W.Y. Ching, Phys. Rev. B 51 (1995) 13023.
[43] J.G. Yu, J.F. Xiong, B. Cheng, S.W. Liu, Appl. Catal. B 60 (2005) 211.
[44] J.G. Yu, H.G. Yu, C.H. Ao, S.C. Lee, J.C. Yu, W.K. Ho, Thin Solid Films 496 (2006) 273.
[45] J.G. Yu, J.F. Xiong, B. Cheng, Y. Yu, J.B. Wang, J. Solid State Chem. 178 (2005) 1968.